nature chemical biology

ARTICLES

https://doi.org/10.1038/s41589-020-0535-8

Check for updates

# TRUPATH, an open-source biosensor platform for interrogating the GPCR transducerome

Reid H. J. Olsen[1,5], Jeffrey F. DiBerto[1,5], Justin G. English[1], Alexis M. Glaudin[1], Brian E. Krumm[1], Samuel T. Slocum[1,2], Tao Che[1], Ariana C. Gavin[1], John D. McCorvy[1,3], Bryan L. Roth[1,2,4]✉ and Ryan T. Strachan[1]✉

**G-protein-coupled receptors (GPCRs) remain major drug targets, despite our incomplete understanding of how they signal through 16 non-visual G-protein signal transducers (collectively named the transducerome) to exert their actions. To address this gap, we have developed an open-source suite of 14 optimized bioluminescence resonance energy transfer (BRET) Gαβγ biosensors (named TRUPATH) to interrogate the transducerome with single pathway resolution in cells. Generated through exhaustive protein engineering and empirical testing, the TRUPATH suite of Gαβγ biosensors includes the first Gα15 and GαGustducin probes. In head-to-head studies, TRUPATH biosensors outperformed first-generation sensors at multiple GPCRs and in different cell lines. Benchmarking studies with TRUPATH biosensors recapitulated previously documented signaling bias and revealed new coupling preferences for prototypic and understudied GPCRs with potential in vivo relevance. To enable a greater understanding of GPCR molecular pharmacology by the scientific community, we have made TRUPATH biosensors easily accessible as a kit through Addgene.**

G-protein-coupled receptors (GPCRs) represent not only the largest family of membrane targets for US Food and Drug Administration (FDA)-approved drugs[1], but are also among the most understudied drug targets in the human genome[1,2]. It is widely appreciated that GPCR ligands can bias receptor activity towards distinct intracellular G-protein and arrestin pathways via a process known as functional selectivity or biased agonism[3,4]. Notably, biased agonists for κ-opioid[5] and μ-opioid[6], β-adrenergic[7] and other receptors[8] may provide therapeutic actions with fewer deleterious side effects[9]. Accordingly, creating biased ligands that activate or attenuate specific G-protein or arrestin signaling pathways is a major area of research for chemical biologists, pharmacologists and drug discovery scientists.

The complex signaling mechanisms that drive the therapeutic efficacy and side effects of GPCR-targeted drugs remain largely unknown[10], complicating efforts to create pathway-specific drugs. This is due, in part, to insufficiently robust and scalable assay platforms to interrogate multiple G proteins with single pathway resolution in cells. Such resolution is key, as GPCRs can activate up to 16 different non-visual G-protein transducers (collectively dubbed the transducerome) with considerable redundancy at the second messenger level. For example, seven Gi/o class proteins are known to inhibit cyclic adenosine monophosphate (cAMP) in cellular assays. A variety of bioluminescence resonance energy transfer (BRET)- and fluorescence resonance energy transfer (FRET)-based assays have been developed for different G-protein family pathways[11,12], although they do not directly measure G-protein activation. Although more direct BRET- and FRET-based assays for measuring the activation of individual G-protein subunits have been employed since 2001[13], no easily accessible and comprehensive set of Gαβγ FRET or BRET probes have been reported[14–19]. Additionally, of those that exist, relatively few have been fully optimized and characterized.

Here, we report the results of a large-scale optimization and validation campaign aimed at developing robust BRET2-based biosensors to measure the activation of non-visual G-protein, a platform that we have dubbed TRUPATH (for G-protein transducer pathways). Specifically, we optimized each component of the Gαβγ heterotrimer (that is, 16 different Gα subunits, 4 major Gβ subunits and 12 Gγ subunits) to develop a single readout biosensor platform covering 14 G-protein pathways. In head-to-head studies, TRUPATH biosensors outperformed first-generation sensors at multiple GPCRs and in different cell lines. Benchmarking studies with TRUPATH biosensors recapitulated previously documented signaling bias and revealed new coupling preferences for prototypic and understudied GPCRs with potential in vivo relevance. To enable a greater understanding of GPCR molecular pharmacology by the scientific community, we have made TRUPATH biosensors easily accessible as a kit through Addgene (https://www.addgene.org/).

## Results

**Optimization of Gα-RLuc8/Gβ/Gγ-GFP2 biosensors.** The proximal steps that initiate G-protein signaling cascades include receptor-mediated guanine nucleotide exchange at the Gα-subunit of the Gαβγ heterotrimer and subsequent dissociation of the heterotrimeric complex. Heterotrimer dissociation ultimately leads to effector activation and downstream cellular responses[20]. A decrease in the resonance energy transfer (RET) between fluorescently (FRET) or luminescently (BRET1 or BRET2) labeled heterotrimer subunits can detect dissociation and has been used as a proxy for

[1]Department of Pharmacology, University of North Carolina Chapel Hill School of Medicine, Chapel Hill, NC, USA. [2]National Institute of Mental Health Psychoactive Drug Screening Program, University of North Carolina Chapel Hill School of Medicine, Chapel Hill, NC, USA. [3]Department of Cell Biology, Neurobiology, and Anatomy, Medical College of Wisconsin, Milwaukee, WI, USA. [4]Division of Chemical Biology and Medicinal Chemistry, Eshelman School of Pharmacy, University of North Carolina, Chapel Hill, NC, USA. [5]These authors contributed equally: Reid H. J. Olsen, Jeffrey F. DiBerto. ✉e-mail: bryan_roth@med.unc.edu; rstracha@email.unc.edu

direct measurements of ligand–receptor transducer coupling[13,15,18] (Supplementary Fig. 1a). Because optimal FRET and BRET probe pairs depend on both the proximity of the donor and acceptor proteins and the orientation of their transition dipole moments (Supplementary Fig. 1b), the de novo design of high-performing Gαβγ sensors is challenging and non-trivial. This is due in part to the diverse conformations and orientations of Gα and Gβγ subunits, especially in their inactive states[21]. Here we chose the variant BRET2, given its increased spectral resolution over BRET1 (~115 nm versus 45–55 nm, respectively). Although high-resolution structures can be used to identify potential regions for inserting donor or acceptor molecules based on proximity constraints, they cannot readily predict the conformational dynamics of the target proteins that might influence resonance energy transfer efficiency. Here, we have combined structure-guided protein engineering with exhaustive experimental refinement to afford optimal Gα-RLuc8 donor and Gβγ-GFP2 acceptor BRET2 pairs for 14 different human G proteins.

To limit the number of Gα-RLuc8 donor chimeras tested, we first targeted the flexible loop regions between the αA-αB and αB-αC helices in the α-helical domain of the Gα-subunit (Supplementary Fig. 1c). Although these regions are amenable to insertion of fluorescent[13,22] and luminescent[15] proteins, varying the insertion site can have unpredictable and sometimes deleterious effects on Gα protein function[23]. Accordingly, we generated between 12 and 20 RLuc8 insertions for each Gα subunit to sample every amino acid position within these loops (Supplementary Fig. 1d). To guide our approach, we relied on published crystal structures or homology models (Supplementary Table 1). Each Gα-RLuc8 chimeric donor was tested alongside standard Gβ1/Gγ2-GFP2 or Gβ1/Gγ1-GFP2 acceptor constructs and an appropriate model GPCR (for example $NT_1R$ neurotensin-1 receptor for Gαq-class G proteins) (Supplementary Fig. 1e). The concentration–response curve for each chimera was then compared to the response of a reference Gα-RLuc8 chimera (that is, RLuc8 inserted after the first lysine in the αA-αB linker domain; insertion of RLuc8 after Lys97 in Gαq was named Gαq(98) RLuc8). This reference site was chosen because of its use in many first-generation FRET, BRET1 or BRET2 Gαβγ biosensors[13,15,23], which also represent the largest documented set so far. Of the top five performing Gα-RLuc8 chimeras, the Gα-RLuc8 that reproducibly exhibited the greatest dynamic range was then advanced to the Gβγ-GFP2 optimization phase (Supplementary Fig. 1f).

Optimal Gβγ-GFP2 acceptors were subsequently identified through stepwise screening of 12 N-terminal Gγ-GFP2 fusions (Gγ1–13) and four wild-type Gβ subunits (Gβ1–4). Experimentally, Gγ screens included the optimal Gα-RLuc8 chimera, a co-precipitated mixture of wild-type Gβ1–4, a single Gγ-GFP2 test construct and a model GPCR (Supplementary Fig. 1g). The Gα-RLuc8/Gγ-GFP2 pair that exhibited the greatest dynamic range was then screened against each of four Gβ subunits (Supplementary Fig. 1h). This stepwise optimization process was repeated for all G proteins to produce the final suite of TRUPATH Gα-RLuc8/Gβγ-GFP2 biosensors (Table 1, Supplementary Fig. 1i and Supplementary Note).

The first fully optimized biosensor was Gαq. We defined the initial set of Gαq-RLuc8 insertions sites to be 98–106 and 116–126 within the loops connecting αA-αB and αB-αC helices, respectively (PDB 3AH8)[24] (Fig. 1a). For this initial screen we used γ1-GFP2 as the acceptor construct given its recent use with Gαq sensors[25] and $NT_1R$ as the model receptor and truncated neurotensin (NT8–13) as the test agonist. RLuc8 insertion positions 119, 122, 123, 125 and 126 produced the greatest responses relative to reference position 98 (boxed, Fig. 1b). RLuc8 insertion at position 125 (Gαq(125)-RLuc8) was confirmed as exhibiting the greatest response magnitude (Fig. 1c) and advanced to the Gγ-GFP2 optimization phase. Screening Gαq(125)-RLuc8 against 12 Gγ-GFP2 chimeras identified Gγ1 and Gγ9 as the most optimal acceptor constructs with Gγ9 slightly outperforming Gγ1 (boxed, Fig. 1d). At the Gβ optimization phase, Gβ3 exhibited a slightly greater net BRET response in conjunction with Gγ9-GFP (boxed, Fig. 1e). As proof of concept, the resultant Gαq biosensor Gαq(125)-RLuc8/Gβ3γ9-GFP2 reported robust activation by a panel of canonically Gαq-coupled receptors (Supplementary Fig. 2a). Finally, we confirmed that RLuc8 insertion did not compromise Gαq(125)-RLuc8 function in HEK293 cells lacking Gαq/11/12/13/s/Olf (HEK293ΔG) proteins[26]. As shown in Supplementary Fig. 2b, $NT_1R$ activated Gαq(125)-RLuc8 with a potency equal to the wild-type Gαq.

**Table 1 | Composition of each heterotrimeric BRET2 biosensor in the TRUPATH suite of reagents**

| Gα | AA position | Gγ-GFP2 | Gβ |
|---|---|---|---|
| i1 | 91 | γ9 | β3 |
| i2 | 91 | γ8 | β3 |
| i3 | 99 | γ9 | β3 |
| oA | 92 | γ8 | β3 |
| oB | 92 | γ8 | β3 |
| Z | 114 | γ1 | β3 |
| Gustducin | 117 | γ1 | β3 |
| sS | 123 | γ9 | β3 |
| sL | 137 | γ1 | β1 |
| Olf | ND | ND | ND |
| Q | 125 | γ9 | β3 |
| 11 | 246 | γ13 | β3 |
| 14 | ND | ND | ND |
| 15 | 245 | γ13 | β3 |
| 12 | 134 | γ9 | β3 |
| 13 | 126 | γ9 | β3 |

Amino acid (AA) position number indicates the position in the Gα protein of the first amino acid of the linker flanking the RLuc8 sequence. ND, 'not determined'; refers to unsuccessful sensor optimization or a failure to produce a functional sensor with any of the designs employed.

The same optimization workflow (Fig. 1 and Supplementary Fig. 1f–i) was successfully applied to other human Gα-subunits (Supplementary Figs. 3–11, 13 and 15–17), including two first-in-class biosensors for Gα15 and GαGustducin. Optimization of Gαi1, Gαi2, Gαi3, GαZ, GαsShort, GαsLong, Gα12 and Gα13 identified new RLuc8 insertion sites that outperformed the reference positions, while the reference constructs for GαoA and GαoB were ultimately the most suitable sites (Table 1). Notably, apart from some of the closely related Gαi-class (Gαi1, Gαi2, GαoA and GαoB) and Gαs isoforms, we did not observe consistent patterns in optimal RLuc8 positioning. This demonstrates that a purely structure-guided or homology-based approach for generating Gα-RLuc8 chimeras is not likely to be successful and that optimal design is non-obvious. We also observed that the optimal Gβγ-GFP2 dimer construct for most Gα-subunits was Gβ3γ9 and not the commonly used Gβ1γ2 or Gβ1γ1 dimers. Ultimately, we found that many combinations of Gβγ-GFP2 (for example, Gβ3γ8 and Gβ3γ1; Table 1) were superior to the acceptor combinations used in published biosensors, further confirming the validity of our empirical, unbiased approach.

We failed to detect substantial basal BRET2 responses or reproducible concentration–response curves for GαOlf, Gα11, Gα14 and Gα15 when inserting RLuc8 within the α-helical domain (Supplementary Figs. 12–15). Using the crystal structure of the guanosine diphosphate (GDP)-bound Gαq/Gβ1γ2 heterotrimer complex (PDB 3AH8), we identified alternative RLuc8 insertion sites, first focusing on Gα11 given its high identity (90%) and

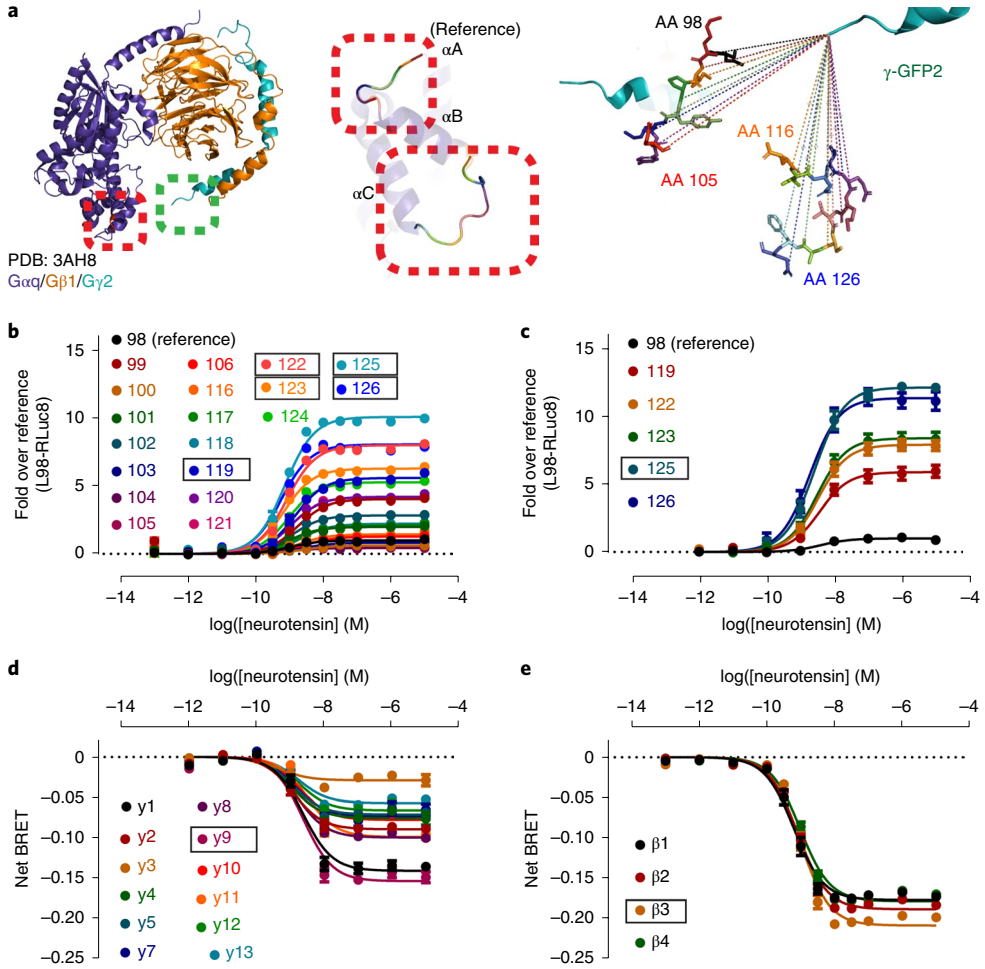


**Fig. 1 | Optimization workflow for the exemplar Gαq biosensor. a–c**, RLuc8 donor positioning. **a**, The inactive Gαq/Gβ1/γ2 crystal structure (PDB 3AH8) defined regions within the α-helical domain (red box) in close proximity to the N terminus of the Gγ-subunit (green box). Twenty Gαq-RLuc8 chimeric proteins were generated between αA-αB and αB-αC helices. **b**, Gαq-RLuc8 chimeras were evaluated in duplicate using the prototypic Gαq-coupled $NT_1R$ neurotensin receptor. Performance was evaluated as fold increase in dynamic range (net BRET2) relative to the reference construct (insertion of RLuc8 after Lys97 in Gαq was named position 98). **c**, The top five RLuc8 positions (119, 122, 123, 125, 126; boxed) were confirmed ($N=3$) and Gαq(125)-RLuc8 was chosen as the optimal chimeric donor (**c**, boxed). **d**, Gγ-GFP2 optimization: the Gαq(125)-RLuc8 chimera was tested alongside each of 12 N-terminally fused Gγ-GFP2 constructs and a co-precipitated mixture of Gβ1–4 subunits. The Gγ9-GFP2 chimera provided the largest signal ($N=3$). **e**, Gβ optimization: Gαq(125)-RLuc8 and Gγ9-GFP2 were used to screen each of four Gβ subunits ($N=3$). Stepwise optimization determined that Gαq(125)-RLuc8/Gβ3γ9-GFP2 was the optimal biosensor composition.

similarity (96%) to Gαq. After excluding residues and regions already interrogated, those with known secondary structures and those within flexible regions of Switch II because of its many sites of contact with the Gβ subunit, we identified a flexible loop region named Switch III that is situated between the β4-strand and the α3-helix of the Ras-like domain (Fig. 2a). The closest Switch III residue to Gγ2 was a glutamic acid at position 241 (E241; Fig. 2a, inset), a conserved amino acid whose backbone carbonyl mediates interactions with regulator of G-protein signaling (RGS) proteins[27] and that is involved in Gα signaling to downstream effectors but has no effect on receptor-mediated guanosine triphosphate (GTP)–GDP exchange, GTP hydrolysis, or physical binding to phosphodiesterases (PDE)[28]. Inserting RLuc8 into this region (Gα11(241)-RLuc8) yielded a chimera that retained wild-type functionality in calcium mobilization assays in HEK293ΔG cells (Supplementary Fig. 2c). We next generated and screened Gα11-RLuc8 constructs spanning the entire Switch III region (Fig. 2b), using Gβ3/Gγ13-GFP2 as a suitable acceptor pair (Supplementary Fig. 13e,f and Fig. 2c). We ultimately identified Gα11(246)-RLuc8/Gβ3γ13-GFP2 as the top-performing biosensor composition (Fig. 2d–f). For completeness, we determined that the Gα11(246)-RLuc8 chimera recapitulated wild-type function in a calcium mobilization assay (Supplementary Fig. 20e). Therefore, Switch III is a novel and fruitful region for Gα-protein engineering.

Targeting Switch III for the remaining G proteins yielded the first functional Gα15 biosensor (Supplementary Fig. 15), but did not yield functional Gα14 (Supplementary Fig. 14e) or GαOlf (Supplementary Fig. 12f, position 244) biosensors. It is unlikely that exogenous Gα14 or GαOlf are non-functional, as overexpression of these subunits activates effectors in HEK293T cells[25,29]. Based on the low basal BRET2 signals for both the α-helical domain (Supplementary Fig. 14b) and Switch III Gα14-RLuc8 chimeras (Supplementary Fig. 14e), and the observation that replacing the entire α-helical domain of Gα14 with that of the Gαq(125)-RLuc8 construct did not produce a functional biosensor (Supplementary Fig. 14f), we surmise that the engineered Gα14 heterotrimer is unstable or dysfunctional, or that Gα14 may exist predominantly dissociated from Gβγ. By contrast, GαOlf-RLuc8 chimeras exhibited good basal BRET2 (Supplementary Fig. 12a–c), but these were not activated by canonically GαOlf-coupled receptors (for example,

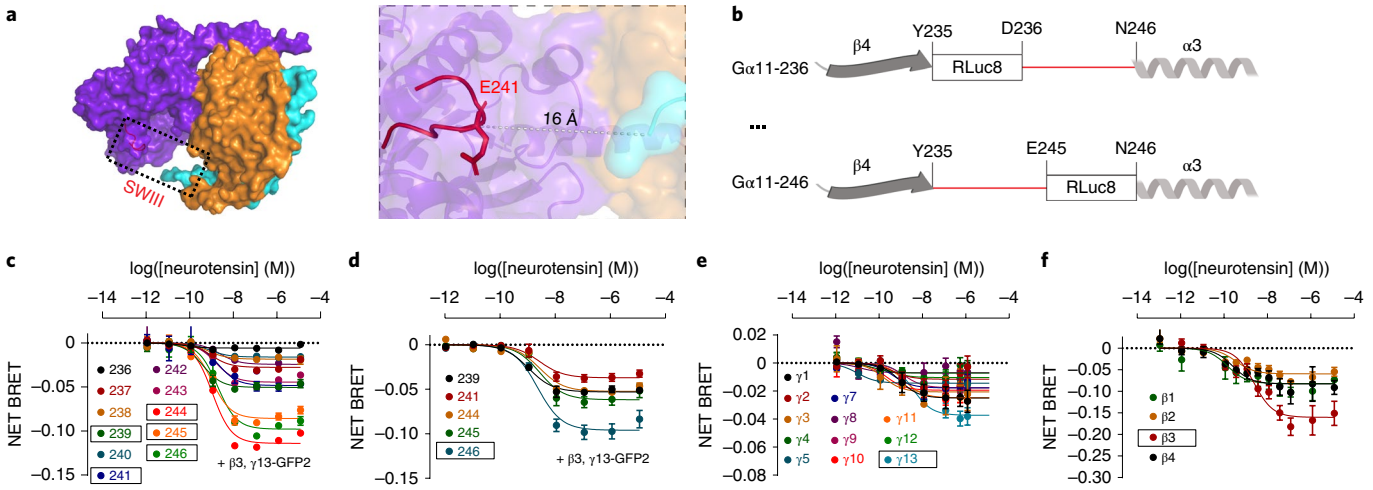


**Fig. 2 | Switch III in the Gα-subunit is a novel region for protein engineering. a**, For challenging G proteins like Gα11, we identified a new site for RLuc8 insertion located between the β4-strand and α3-helix of the Ras-like domain (denoted Switch III (SWIII), dashed box). The closest residue in the Gα11 model to the Gγ N terminus was Glu241 (inset). **b**, Schematic delineating the Switch III region and RLuc8 insertion sites for Gα11. **c**, Donor optimization results for Gα11 Switch III RLuc8 insertions ($N=1$, two technical replicates; the top five positions are 239, 241, 244, 245, 246 (boxed)). **d**, Gα11(246)-RLuc8 was confirmed as the optimal donor chimera ($N=3$). **e**, Gγ13-GFP2 (boxed) was selected as the optimal BRET2 acceptor ($N=3$). **f**, Gβ3 was selected as the optimal Gβ subunit, yielding Gα11(246)-RLuc8/Gβ3γ13-GFP2 as the final biosensor composition ($N=3$). Data are presented as mean values ± s.e.m.

adenosine 2A, Gs-DREADD, or dopamine D1) (Supplementary Fig. 12a–c). Attempts to replicate recently published BRET2 biosensors for GαOlf[16] were similarly unsuccessful (Supplementary Fig. 12d,e). Forced activation by treatment with cholera toxin produced an expected decrease in Gαs-mediated BRET2, but produced an increase in GαOlf BRET2 (Supplementary Fig. 12f,g), despite a shared sensitivity and mechanism of action. The reasons for this remain unclear but probably reflect a stable, yet non-functional GαOlf heterotrimer.

**Characterization of optimized G-protein biosensors.** To gauge their relative performance we compared TRUPATH biosensors with published first-generation biosensors[15]. In the case of G proteins not part of this original set, equivalent RLuc8 chimeras were used. Using multiple model receptor systems, each TRUPATH biosensor outperformed its comparator with statistically significant improvements ranging from 1.5- to ~100-fold (Fig. 3a–j, Supplementary Fig. 18a,b,d,e and Supplementary Table 2), with the median and mean improvement being 7.8- and 20.5-fold, respectively. As during the development process, GαOlf and Gα14 sensors failed to produce a concentration–response curve (Supplementary Fig. 18c,f). To compensate for any receptor-dependent effects, we also performed a head-to-head comparison using the $AT_1R$ angiotensin II receptor, as previously reported[15]. As shown in Supplementary Fig. 19, TRUPATH biosensors statistically outperformed first-generation sensors at most pathways. Significantly, AngII-mediated activation of Gα12 was completely missed by a first-generation biosensor but yielded a robust response at the corresponding TRUPATH sensor (Supplementary Fig. 19i), suggesting that $AT_1R$ is not biased against Gα12, as previously determined[15]. Together, these comparisons demonstrate the enhanced performance and importance of using optimized G-protein biosensors.

We next determined if TRUPATH biosensors could detect inverse agonism, given that the baseline BRET2 response reflects the equilibrium of associated/dissociated Gαβγ heterotrimer. For these experiments we chose the Gi-coupled cannabinoid-1 receptor ($CB_1R$), which exhibits high constitutive activity[30]. As shown in Supplementary Fig. 20a for our optimized Gαi3 biosensor, the inverse-agonist rimonabant caused a very large decrease in normalized $CB_1R$ constitutive activity, while the full agonist WIN 55,212-2 produced a comparably weaker increase in activity (Supplementary Table 3). These data support the sensitive detection of inverse agonism using TRUPATH biosensors.

Ligand parameters of potency (half-maximum effective concentration, $EC_{50}$) and efficacy (the degree to which a ligand produces a maximal response, $E_{max}$) are greatly modulated by the level of receptor reserve and by amplification of the stimulus–response cascade, both of which complicate efforts to accurately characterize ligand pharmacology and quantify ligand bias[31]. Because heterotrimeric BRET2 sensors measure pathway activation proximal to the receptor, we posited that signal amplification should be minimal, although receptor reserve could be operative. To test this, we eliminated spare receptors via receptor-alkylation. We found that depletion of the μ-opioid receptor (μOR) with increasing concentrations (0–30 nM) of the irreversible antagonist β-funaltrexamine[32] (β-FNA) significantly reduced the $E_{max}$ of the full agonist DAMGO, with a modest effect on potency (Supplementary Fig. 20b–d and Supplementary Table 3). Specifically, we identified a trend of decreasing $pEC_{50}$ values with increasing β-FNA concentration ($F(1,52)=6.793$, $P=0.0119$), but with a small effect size ($r^2=0.1005$), suggesting that the observed effect is likely to be real but small. Conversely, the effect of increasing concentrations of β-FNA on the maximum response was large and immediate ($F(1,52)=180.6$, $P<0.0001$; $r^2=0.7502$). Taken together, these data suggest that TRUPATH assays exhibit minimal amplification and/or receptor reserve under the conditions used here. In direct support of this, radioligand binding assays confirmed receptor density to be quite modest (219 ± 5 fmol $mg^{-1}$; mean ± s.e.m., $n=3$). Thus, TRUPATH biosensors provide accurate measurements of ligand potency and efficacy without the need for post-processing methods[33], which is ideal for quantifying functional selectivity across the human transducerome.

We also controlled for the possibility that Gα-RLuc8 chimeras were functionally compromised by comparing a subset of Gα-RLuc8 sensors covering three major effector classes to their wild-type counterparts in standard second messenger assays. The Gαq, Gα11, Gα15, Gαi3, GαZ and Gαs TRUPATH sensors performed similarly to, and were statistically indistinguishable from, their wild-type counterparts (Supplementary Figs. 2b,c and 20e–h and Supplementary Table 3), demonstrating that our biosensors recapitulate wild-type functionality.

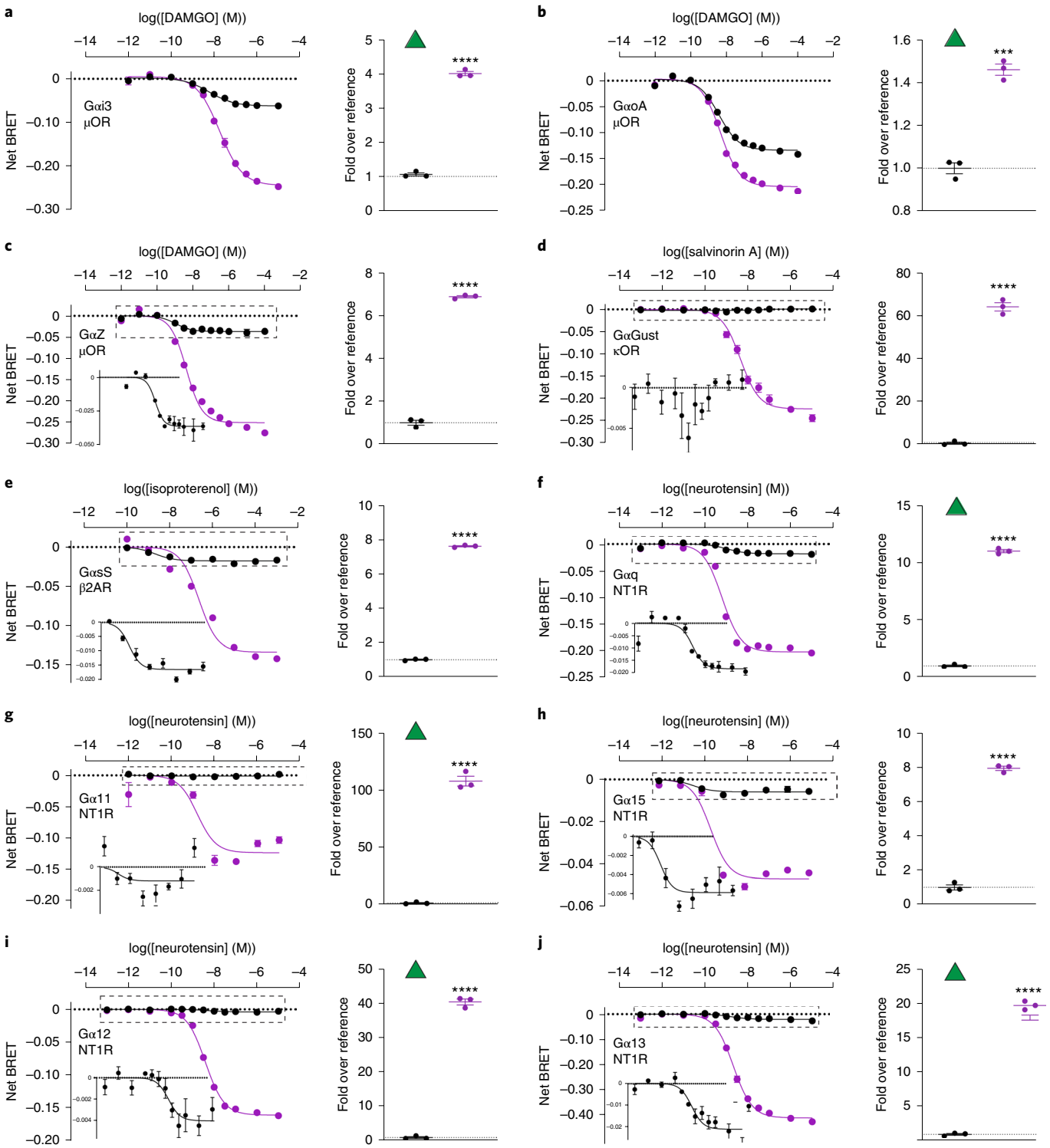


**Fig. 3 | Head-to-head comparisons of TRUPATH biosensors to first-generation BRET2 biosensors.** TRUPATH biosensors are shown in purple and first-generation biosensors are shown in black (pathways compared to published biosensors are indicated by green triangles; equivalent RLuc8 positioning was used for previously undisclosed G proteins). The dot plots show the fold difference in amplitude between comparator and TRUPATH biosensors (*two-tailed *t*-test, $P < 0.05$). Additional comparisons are made in Supplementary Fig. 18. **a**, (Comparator) Gαi3(92)-RLuc8/Gβ1γ2-GFP2 < (TRUPATH) Gαi3(99)-RLuc8/Gβ3γ9-GFP2, $P < 0.0001$. **b**, (Comparator) GαoA(92)-RLuc8/Gβ1γ2-GFP2 < (TRUPATH) GαoA(92)-RLuc8/Gβ3γ8-GFP2, $P = 0.0007$. **c**, (Comparator) GαZ(92)-RLuc8/Gβ1γ2-GFP2 < (TRUPATH) GαZ(114)-RLuc8/Gβ3γ1-GFP2, $P < 0.0001$. **d**, (Comparator) GαGustducin(92)-RLuc8/Gβ1γ2-GFP2 < (TRUPATH) GαGustducin(117)-RLuc8/Gβ3γ1-GFP2, $P < 0.0001$. **e**, (Comparator) GαsS(100)-RLuc8/Gβ1γ1-GFP2 < (TRUPATH) GαsS(123)-RLuc8/Gβ3γ9-GFP2, $P < 0.0001$. **f**, (Comparator) Gαq(98)-RLuc8/Gβ1γ1-GFP2 < (TRUPATH) Gαq(125)-RLuc8/Gβ3γ9-GFP2, $P < 0.0001$. **g**, (Comparator) Gα11(98)-RLuc8/Gβ1γ1-GFP2 < (TRUPATH) Gα11(246)-RLuc8/Gβ3γ13-GFP2, $P < 0.0001$. **h**, (Comparator) Gα15(101)-RLuc8/Gβ1γ2-GFP2 < (TRUPATH) Gα15(245)-RLuc8/Gβ3γ13-GFP2, $P < 0.0001$. **i**, (Comparator) Gα12(115)-RLuc8/Gβ1γ2-GFP2 < (TRUPATH) Gα12(134)-RLuc8/Gβ3γ9-GFP2, $P < 0.0001$. **j**, (Comparator) Gα13(107)-RLuc8/Gβ1γ2-GFP2 < (TRUPATH) Gα13(126)-RLuc8/Gβ3γ9-GFP2, $P < 0.0001$. Data are presented as mean values ± s.e.m. from three biological replicates. Raw values are reported in Supplementary Table 2.

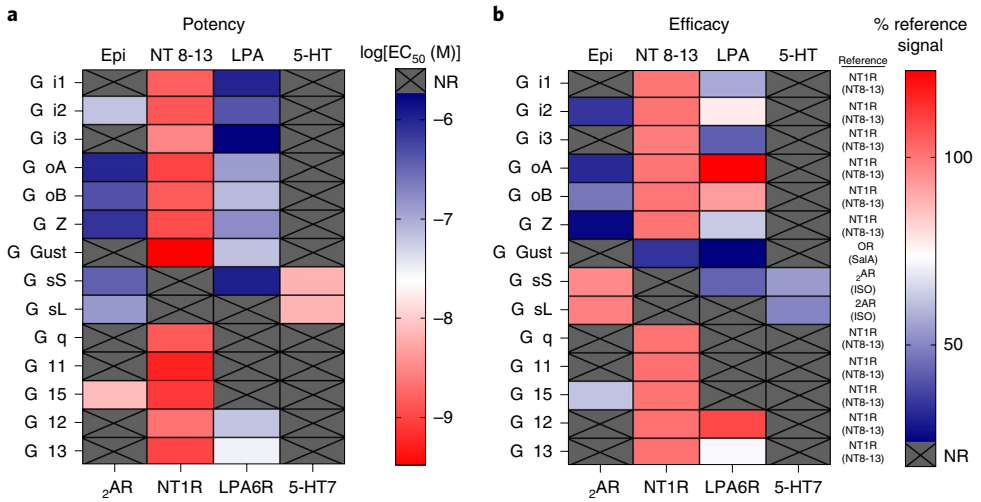


**Fig. 4 | TRUPATH screens of prototypic and understudied GPCRs reveal varying degrees of transducer promiscuity.** Transducerome profiles of endogenous agonists for prototypic receptors ($\beta_2$AR β-adrenergic and $NT_1$R neurotensin) and understudied receptors ($LPA_6$ LPA and 5-$HT_7$ serotonin) demonstrate varying degrees of promiscuity. **a**, Potency (log($EC_{50}$)) values are non-uniform across the transducerome for receptor–ligand pairs. **b**, Relative amplitude ($E_{max}$ or efficacy) of agonist-induced stimulation of TRUPATH biosensors is frequently non-uniform for a given receptor–ligand pair. Data are presented as mean values ± s.e.m. Heatmap values represent mean values; NR, no response, presented as a gray square. Mean values, standard error and replicate numbers are reported in Supplementary Dataset 1. Statistically significant differences between efficacies and potencies are reported in Supplementary Datasets 2 and 3, respectively.

**Interrogating the human G protein transducerome.** TRUPATH biosensors were developed to comprehensively profile GPCR coupling preferences. We profiled a panel of well-studied and understudied GPCRs and their endogenous ligands in HEK293T (Fig. 4) and Chinese hamster ovary (CHO) cells (Supplementary Fig. 22). To account for variation between experiments, the $NT_1$R neurotensin receptor served as a reference standard for all G proteins except GαGustducin and Gαs isoforms, for which the κ-opioid receptor (κOR) and $\beta_2$AR were used, respectively.

We first profiled the prototypic $\beta_2$AR and its endogenous agonist epinephrine (Epi) in HEK293T cells. In addition to the expected coupling to canonical Gαs-family proteins, modest coupling to Gαi-class transducers was detected, as previously reported (Fig. 4 and Supplementary Fig. 21a). We observed remarkable restriction of epinephrine activity to a subset of Gαi-class proteins including Gαi2, GαoA, GαoB and GαZ, suggesting that the receptor-transducer interface differentiates between functionally similar G proteins. We confirmed that activation of the Gαi2 TRUPATH sensor was due to exogenous $\beta_2$AR and not endogenous adrenergic receptors by substituting pcDNA for $\beta_2$AR and treating with epinephrine or the $\alpha_2$-adrenergic receptor-selective agonist clonidine (Supplementary Fig. 21b). Similarly, the $\beta_2$AR-selective agonist isoproterenol activated Gαi2 (Supplementary Fig. 21b). In confirmation of earlier reports[34], the epinephrine-activated $\beta_2$ARs also coupled to Gα15 with moderate efficacy (Fig. 4b) and greater potency (Fig. 4a) compared to other G-protein pathways (Supplementary Fig. 21a and Supplementary Datasets 1–3). Accordingly, Epi elicited calcium responses in HEKΔG cells that were blocked by the βAR antagonist alprenolol (Supplementary Fig. 21c).

We next profiled the well-studied ($NT_1$R) and less thoroughly interrogated ($LPA_6$ lysophosphatidic acid and 5-$HT_7$ serotonin) receptors using their respective endogenous agonists neurotensin (8–13), 1-oleoyl lysophosphatidic acid (LPA) and serotonin (5-HT). The $NT_1$R coupled to nearly all G proteins except for the Gαs isoforms (Fig. 4b). By contrast, $LPA_6$R coupling was restricted to subsets of Gαi/o isoforms, Gα12/13 and minimally to GαsShort. Although the discrepancy between GαsShort and GαsLong coupling was notable as they are isoforms, the low solubility of LPA precluded testing at higher concentrations that might have otherwise revealed weak coupling to GαsLong. The 5-$HT_7$ receptor exhibited the greatest selectivity of the four receptors, coupling exclusively to both Gαs isoforms (Fig. 4b).

We controlled for cell-type differences in TRUPATH biosensor performance by profiling endogenous agonists at the $\beta_2$AR and $NT_1$R in CHO cells. As shown in Supplementary Fig. 22 (values reported in Supplementary Table 5), we reproduced primary coupling of the $\beta_2$AR to GαsShort, GαsLong and Gα15; weaker secondary coupling to Gi/o-class proteins was not observed, which we attributed to lower expression of BRET2 biosensor components as we observed a consistently reduced luminescent signal in these experiments. By contrast, we reproduced the extreme promiscuity of $NT_1$R in CHO cells originally seen in HEK293T cells (Fig. 4). Altogether, the increased transfection efficiency or greater expression of biosensor components in HEK293T cells appears to confer greater sensitivity to detect weaker coupling events and remains the preferred cell system for TRUPATH profiling.

**Large-scale transducerome drug screening.** TRUPATH biosensors are ideally suited for screening chemically diverse compounds at a single receptor across the human G-protein transducerome. The κOR was selected because of renewed interest in identifying κOR-targeted therapies[5] and its diverse physiological effects including analgesia, anxiety, itch and hallucinations.

Traditional methods for quantifying ligand–receptor transducer bias[35] account for differences between the pathways (for example, arrestin versus G protein), but are not readily scaled to interpret multidimensional data of this type. Specifically, transduction coefficients $\left(\log\left(\frac{E_{max}}{EC_{50}}\right)\right)$ are inappropriate for scenarios involving partial agonists and when the reference agonist is not maximally efficacious across all pathways tested[35], which is particularly relevant as TRUPATH assays experience minimal signal amplification and are comprehensive. Transduction coefficients also mask the individual contributions of $E_{max}$ and $EC_{50}$ to bias, which are important considerations when developing affinity- or efficacy-biased ligands[10] and for building detailed structure–activity relationships. Here, we

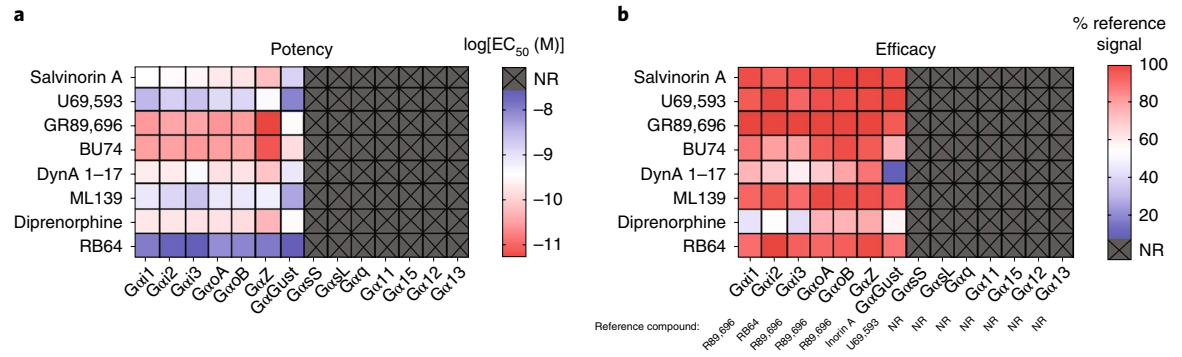


**Fig. 5 | TRUPATH screens of κOR agonists reveal unappreciated transducer-selective effects on potency and efficacy. a**,**b**, TRUPATH heatmaps demonstrate how a panel of κOR agonists engage Gαi/o-class transducers with varying potency (**a**) and efficacy (**b**). Most ligands exhibit enhanced (GαZ) and diminished (GαGustducin) potencies relative to other G-protein transducers. Although many ligands activated all transducers with equal efficacy (salvinorin A, U69,593, GR89,696, ML139 and RB64), others exhibited efficacy bias (BU74, dynorphin A and diprenorphine). Heatmap colors represent mean log($EC_{50}$) and normalized efficacy values; NR, no response, presented as a gray square. Mean values, standard error and *N* are reported in Supplementary Table 4. Statistical analyses of transducer-specific comparisons are reported in Supplementary Datasets 4 (efficacy), 5 (potency), and 6 (transduction coefficients).

consider potency and efficacy (reported in Supplementary Table 4) as separate contributing factors to a ligand's overall manifestation of signaling bias.

The κOR transducer coupling profile for this ligand set was entirely restricted to the Gαi/o effector class, within which we detected a statistically significant range of potency (Fig. 5a) and efficacy (Fig. 5b) values (Supplementary Table 4 and Supplementary Datasets 4–6). This supports our assertion that distinctions in signaling preferences or functional selectivity exist for even the most well-studied receptor systems when screening the transducerome. Specifically, a recurring pattern for many κOR ligands was greater potency at GαZ and weaker potency at GαGustducin (Fig. 5a), which we do not attribute to artefacts of a particular biosensor as this pattern did not extend to all the ligands and receptors examined here. For example, at the $\beta_2$AR receptor, epinephrine exhibited significantly greater potency (120-fold) for the Gα15 pathway relative to Gαi2, a difference that was not observed between these same transducers at $NT_1R$ (Fig. 4a and Supplementary Datasets 1 and 3). Additionally, during the optimization and validation stages of the project we observed enhanced potency of the μ-opioid receptor (μOR) agonist DAMGO at GαZ relative to Gαi3, which was consistent in both BRET2 (Supplementary Figs. 5d and 8d) ($t(4) = 10.11$, $P = 0.0005$) and GloSensor cAMP assays ($t(4) = 14.20$, $P = 0.0001$) (Supplementary Fig. 20g and Supplementary Table 3).

Salvinorin A, U69,593, GR89696, ML139 and RB64 exhibited uniform efficacies across transducers (Fig. 5b, Supplementary Fig. 23 and Supplementary Dataset 4), whereas other ligands exhibited a range of partial agonism between G-protein pathways (Fig. 5b and Supplementary Dataset 4) that varied from small (BU74, Fig. 5b and Supplementary Fig. 23d) to more extreme differences (diprenorphine, Fig. 5b and Supplementary Fig. 23g). Remarkably, the endogenous agonist dynorphin A (1–13)—a relatively efficacious partial agonist at most transducers—was nearly inactive at GαGustducin (Fig. 5b and Supplementary Fig. 23e). Notably, the strongly G protein-biased κOR ligand RB64[5,36] exhibited the least variation in both potency and efficacy across the transducerome (Fig. 5b and Supplementary Fig. 23h).

We endeavored to expand the pharmacologist's toolkit and make readily available an assay platform that enables deep biological insight. Although our assay identifies sets of possible coupling events, the question of biological relevance remains 'How likely is in vitro coupling to translate in vivo?' In a proof-of-concept experiment, we tested the in vivo relevance of our unanticipated finding that the κOR robustly activates the taste receptor transducer GαGustducin (Fig. 5). It was previously reported that activation of a chemogenetic κOR mutant (Ro1) in TAS2R-expressing cells of the tongue mediated bitter taste perception in mice[37]. It was inferred that Ro1, like endogenous TAS2Rs, signaled through GαGustducin to produce this response. Using our GαGustducin biosensor, we confirmed that both the wild-type κOR and the chemogenetic κOR Ro1 activated canonical Gαi3 and novel GαGustducin transducers to a similar extent (Supplementary Fig. 24a,b, respectively). These data provide the first mechanistic support for the aversive behavioral response observed by Mueller and others[37] and suggest that in vitro profiles can translate to the in vivo setting.

## Discussion

Here, we present the TRUPATH suite of 14 optimized BRET2 biosensors (Table 1 and Supplementary Note) that affords near complete coverage of the human G-protein transducerome with enhanced dynamic range compared to first-generation sensors[15]. Although some first-generation BRET2 Gα-RLuc8 chimeras performed reasonably well in our hands (for example, GαoA and GαoB; Fig. 3 and Supplementary Figs. 6, 7 and 18), others failed to report reliable or substantial dynamic ranges (for example, Gs, G11, G12 and G13; Fig. 3 and Supplementary Figs. 10, 11, 13, 16 and 17). Even related transducers, such as the highly homologous Gαq and Gα11 proteins, showed distinctions regarding their performance and amenability to protein engineering (Figs. 2 and 3 and Supplementary Fig. 13). It is thus likely that even small differences in amino acid composition have unpredictable effects on structure or conformational dynamics that are not predicted from their primary sequences or structures. These issues, together with a general pattern of suboptimal performance of many published constructs[16,18], support the rigorous empirical process deployed here to develop TRUPATH biosensors. More broadly, the non-obvious nature of optimal donor–acceptor positioning probably means that a similarly exhaustive approach would benefit the engineering of other RET systems.

Although much has been done to elucidate the molecular and structural basis for arrestinergic versus G-protein signal transduction[38], as well as the physiological significance of these divergent pathways[6], relatively little is known about the consequences of 'non-canonical' G-protein signaling. Thus, similar to the 'dark' regions of the genome[2], the transducerome profiles of most GPCRs remain unexplored, which probably conceals fundamental biology and new therapeutic approaches. It is a matter of observation that similar Gα isoforms exhibit diverse expression patterns ranging from largely ubiquitous[39] to tissue-restricted[40]. The selective signal

transduction profiles of different ligands provide additional layers of complexity to tissue-specific signal transduction and, potentially, afford new opportunities for drug discovery. Although the biological relevance of these Gα-biased signaling events remains to be established in target tissues and organs, what is clear from this study and others[41] is that GPCRs are more promiscuous in their coupling preferences than previously imagined. Whether this 'switching' of Gα-coupling for GPCRs arises as a consequence of modifications such as phosphorylation[42] or is an intrinsic property of a receptor–ligand system, it is evident that much can be learned from a detailed exploration of the transducerome.

The recent work of Sandhu and others[43] used molecular dynamics simulations and Gα C-terminal peptides to show that GPCRs possess latent intracellular G-protein-binding cavities with varying propensities to bind cognate and non-cognate G proteins. Within this framework, promiscuously coupled receptors like the $NT_1R$ neurotensin receptor tested here are likely to have latent binding cavities with energetically favorable hotspots that attract many G-protein C termini to yield tight and productive coupling. Conversely, highly selective GPCRs like the 5-$HT_7$ serotonin receptor probably have latent cavities optimized for strong interactions with one or a few G proteins. A contemporaneous study by Okashah and others[44] looked at the coupling of 12 C-terminal Gα chimeras and four full-length G proteins, from which they derived universal guidelines for G-protein coupling; for example, Gαi-coupled receptors are less promiscuous than Gαs- and Gαq-coupled receptors, amongst others. However, from the small number of transducerome profiles generated here (Fig. 4), we could not corroborate these general guidelines. Specifically, we failed to observe universal Gαi1 coupling (for example, 5-$HT_7$), Gαq coupling for Gs-coupled receptors (for example, 5-$HT_7$ and $\beta_2$AR) and restricted coupling preferences for all Gαi1-coupled receptors (for example, $NT_1R$). These differences probably reflect our use of full-length G proteins and a readout that requires G protein activation (that is, dissociation or rearrangement of the heterotrimeric sensor). By contrast, both of the above studies relied mainly on Gα C termini to drive coupling, which does not account for the influence of the Gα subunit core[44]. Moreover, the formation of stable complexes between agonist-occupied receptors and nucleotide-free G proteins is probably detecting weak secondary coupling that is too inefficient to register as activation in our assay[44].

The optimized heterotrimer compositions for each Gα protein might shed light on endogenous Gβ and Gγ subunit preferences. Indeed, reports have suggested preferred combinations of Gα subunits and specific Gβγ dimers (for example, between GαOlf and Gβ2 and Gγ7[45]). However, a surprisingly limited number of non-canonical Gβγ combinations were the preferred acceptors for most Gα-RLuc8 donors (Table 1). Given that TRUPATH sensor compositions were selected for maximal RET efficiency, it is likely that these biosensor compositions do not represent preferred endogenous heterotrimers, but instead reflect optimal subunit positioning and/or complex stability for maximal RET. This predicts that targeting different regions of the Gα for RLuc8 insertion would yield region-specific Gβγ dimer preferences. Indeed, Gβ3 and Gγ8-GFP2 or Gγ9-GFP2 were the preferred partners for nearly all BRET2 biosensors when RLuc8 was inserted within the Gα α-helical domain. By contrast, RLuc8 insertion within the newly targeted Switch III region of Gα11 and Gα15 selected exclusively for the Gβ3Gγ13-GFP2 dimer. Related to this, it is possible that the different TRUPATH Gαβγ combinations chosen during optimization influence receptor coupling preferences. We find this unlikely, however, considering our ability to reproduce the canonical coupling preferences and previously reported bias for the GPCRs tested here. Furthermore, we identified non-canonical coupling of the $\beta_2$AR to Gα15 via the TRUPATH Gα15 biosensor (Gα15(245)-RLuc8/Gβ3γ13-GFP2) and then verified this coupling via cell-based calcium assays in the absence of exogenous Gβ3Gγ13 (Supplementary Fig. 21c). We have made available (through Addgene) all four Gβ and all 12 Gγ-GFP constructs to accommodate the use of other heterotrimer combinations.

It is worth mentioning that, not unlike other cell-based platforms, TRUPATH biosensors identify the potential for biased agonism for any given ligand-GPCR pair. How this bias translates to a physiological response in the target cell or tissue (that is, how the cell interprets this 'stimulus') is uncertain, as it depends on expression of the requisite signal transduction machinery. Thus, combining TRUPATH profiling with multi-omics strategies could enhance our ability to predict the in vivo consequences of in vitro bias profiles.

In conclusion, the open-source TRUPATH platform represents the most robust, complete and thoroughly documented suite of Gαβγ-based GPCR signaling biosensors available so far. Each biosensor represents either a novel assay for a previously untargeted G-protein pathway (Gα15 and GαGustducin) or, to our knowledge, the most optimized heterotrimer-based BRET2 sensor for previously documented pathways[14,15]. We documented each step of the development and optimization process to encourage adoption of these tools as a common component in the GPCR screening toolkit. Screening tools such as these that provide single pathway resolution will empower consistent and reliable measurements reflective of true signaling preferences. Such insights will undoubtedly accelerate efforts to illuminate the druggable GPCRome[8,46,47] and to understand the consequences of biased G-protein signaling.

## Online content

Any Nature Research reporting summaries, source data, extended data, supplementary information, acknowledgements, peer review information; details of author contributions and competing interests; and statements of data and code availability are available at https://doi.org/10.1038/s41589-020-0535-8.

Received: 15 June 2019; Accepted: 30 March 2020;
Published online: 04 May 2020

## References

1. Kroeze, W. K. et al. PRESTO-TANGO: an open-source resource for interrogation of the druggable human GPCR-ome. *Nat. Struct. Mol. Biol.* **22**, 362–369 (2015).
2. Rodgers, G. et al. Glimmers in illuminating the druggable genome. *Nat. Rev. Drug Discov.* **17**, 301–302 (2018).
3. Roth, B. L. & Chuang, D.-M. Multiple mechanisms of serotonergic signal transduction. *Life Sci.* **41**, 1051–1064 (1987).
4. Urban, J. D. et al. Functional selectivity and classical concepts of quantitative pharmacology. *J. Pharmacol. Exp. Ther.* **320**, 1–13 (2007).
5. White, K. L. et al. The G protein-biased κ-opioid receptor agonist RB-64 is analgesic with a unique spectrum of activities in vivo. *J. Pharm. Exp. Ther.* **352**, 98–109 (2015).
6. Manglik, A. et al. Structure-based discovery of opioid analgesics with reduced side effects. *Nature* **537**, 185–190 (2016).
7. Wisler, J. W. et al. A unique mechanism of β-blocker action: carvedilol stimulates β-arrestin signaling. *Proc. Natl Acad. Sci. USA* **104**, 16657–16662 (2007).
8. Wacker, D., Stevens, R. C. & Roth, B. L. How ligands illuminate GPCR molecular pharmacology. *Cell* **170**, 414–427 (2017).
9. Viscusi, E. R. et al. A randomized, phase 2 study investigating TRV130, a biased ligand of the μ-opioid receptor, for the intravenous treatment of acute pain. *Pain* **157**, 264–272 (2016).
10. Kenakin, T. Biased receptor signaling in drug discovery. *Pharm. Rev.* **71**, 267–315 (2019).
11. Masuho, I., Martemyanov, K. A. & Lambert, N. A. in *G Protein-Coupled Receptors in Drug Discovery*: *Methods and Protocols* vol. 1335 (ed. Filizola, M.) 107–113 (Springer, 2015).
12. Wan, Q. et al. Mini G protein probes for active G protein-coupled receptors (GPCRs) in live cells. *J. Biol. Chem.* **293**, 7466–7473 (2018).
13. Janetopoulos, C., Jin, T. & Devreotes, P. Receptor-mediated activation of heterotrimeric G-proteins in living cells. *Science* **291**, 2408–2411 (2001).
14. Busnelli, M. et al. Functional selective oxytocin-derived agonists discriminate between individual G protein family subtypes. *J. Biol. Chem.* **287**, 3617–3629 (2012).

15. Saulière, A. et al. Deciphering biased-agonism complexity reveals a new active AT1 receptor entity. *Nat. Chem. Biol.* **8**, 622–630 (2012).
16. Yano, H. et al. Development of novel biosensors to study receptor-mediated activation of the G-protein α subunits $G_s$ and $G_{olf}$. *J. Biol. Chem.* **292**, 19989–19998 (2017).
17. Adjobo-Hermans, M. J. et al. Real-time visualization of heterotrimeric G protein Gq activation in living cells. *BMC Biol.* **9**, 32 (2011).
18. Mastop, M. et al. A FRET-based biosensor for measuring Gα13 activation in single cells. *PLoS ONE* **13**, e0193705 (2018).
19. van Unen, J. et al. A new generation of FRET sensors for robust measurement of Gαi1, Gαi2 and Gαi3 activation kinetics in single cells. *PLoS ONE* **11**, e0146789 (2016).
20. Gether, U. & Kobilka, B. K. G protein-coupled receptors. II. Mechanism of agonist activation. *J. Biol. Chem.* **273**, 17979–17982 (1998).
21. Smrcka, A. V. et al. NMR analysis of G-protein βγ subunit complexes reveals a dynamic Gα-Gβγ subunit interface and multiple protein recognition modes. *Proc. Natl Acad. Sci. USA* **107**, 639–644 (2010).
22. Hughes, T. E., Zhang, H., Logothetis, D. E. & Berlot, C. H. Visualization of a functional $Gα_q$-green fluorescent protein fusion in living cells. Association with the plasma membrane is disrupted by mutational activation and by elimination of palmitoylation sites, but not be activation mediated by receptors or $AlF_4^-$. *J. Biol. Chem.* **276**, 4227–4235 (2001).
23. Gibson, S. K. & Gilman, A. G. Giα and Gβ subunits both define selectivity of G protein activation by α2-adrenergic receptors. *Proc. Natl Acad. Sci. USA* **103**, 212–217 (2006).
24. Nishimura, A. et al. Structural basis for the specific inhibition of heterotrimeric $G_q$ protein by a small molecule. *Proc. Natl Acad. Sci. USA* **107**, 13666–13671 (2010).
25. Schrage, R. et al. The experimental power of FR900359 to study $G_q$-regulated biological processes. *Nat. Commun.* **6**, 10156 (2015).
26. Grundmann, M. et al. Lack of β-arrestin signaling in the absence of active G proteins. *Nat. Commun.* **9**, 341 (2018).
27. Tesmer, J. J., Berman, D. M., Gilman, A. G. & Sprang, S. R. Structure of RGS4 bound to $AlF_4^-$-activated $G_{i\alpha1}$: stabilization of the transition state for GTP hydrolysis. *Cell* **89**, 251–261 (1997).
28. Li, Q. & Cerione, R. A. Communication between Switch II and Switch III of the transducin α subunit is essential for target activation. *J. Biol. Chem.* **272**, 21673–21676 (1997).
29. Kwan, D. H. T., Yung, L. Y., Ye, R. D. & Wong, Y. H. Activation of Ras-dependent signaling pathways by G14-coupled receptors requires the adaptor protein TPR1. *J. Cell. Biochem.* **113**, 3486–3497 (2012).
30. Felder, C. C. et al. Comparison of the pharmacology and signal transduction of the human cannabinoid CB1 and CB2 receptors. *Mol. Pharmacol.* **48**, 443–450 (1995).
31. Kenakin, T. Gaddum Memorial Lecture 2014: Receptors as an evolving concept: from switches to biased microprocessors. *Br. J. Pharmacol.* **172**, 4238–4253 (2015).
32. Rothman, R. B. et al. β-FNA binds irreversibly to the opiate receptor complex: in vivo and in vitro evidence. *J. Pharmacol. Exp. Ther.* **247**, 405–416 (1988).
33. Kenakin, T. Functional selectivity and biased receptor signaling. *J. Pharm. Exp. Ther.* **336**, 296–302 (2011).
34. Innamorati, G. et al. Heterotrimeric G proteins demonstrate differential sensitivity to β-arrestin dependent desensitization. *Cell. Signal.* **21**, 1135–1142 (2009).
35. Kenakin, T., Watson, C., Muniz-Medina, V., Christopoulos, A. & Novick, S. A simple method for quantifying functional selectivity and agonist bias. *ACS Chem. Neurosci.* **3**, 193–203 (2011).
36. White, K. L. et al. Identification of novel functionally selective κ-opioid receptor scaffolds. *Mol. Pharmacol.* **85**, 83–90 (2014).
37. Mueller, K. L. et al. The receptors and coding logic for bitter taste. *Nature* **434**, 225–229 (2005).
38. Wacker, D. et al. Crystal structure of an LSD-bound human serotonin receptor. *Cell* **168**, 377–389.e12 (2017).
39. Garibay, J. L. R. et al. Analysis by mRNA levels of the expression of six G protein α-subunit genes in mammalian cells and tissues. *Biochim. Biophys. Acta Mol. Cell Res.* **1094**, 193–199 (1991).
40. Hinton, D. R. et al. Novel localization of a G protein, Gz-α, in neurons of brain and retina. *J. Neurosci.* **10**, 2763–2770 (1990).
41. Inoue, A. et al. Illuminating G-protein-coupling selectivity of GPCRs. *Cell* **177**, 1933–1947.e25 (2019).
42. Daaka, Y., Luttrell, L. M. & Lefkowitz, R. J. Switching of the coupling of the β2-adrenergic receptor to different G proteins by protein kinase A. *Nature* **390**, 88–91 (1997).
43. Sandhu, M. et al. Conformational plasticity of the intracellular cavity of GPCR-G-protein complexes leads to G-protein promiscuity and selectivity. *Proc. Natl Acad. Sci. USA* **116**, 11956–11965 (2019).
44. Okashah, N. et al. Variable G protein determinants of GPCR coupling selectivity. *Proc. Natl Acad. Sci. USA* **116**, 12054–12059 (2019).
45. Hervé, D. Identification of a specific assembly of the G protein golf as a critical and regulated module of dopamine and adenosine-activated cAMP pathways in the striatum. *Front Neuroanat.* **5**, 48 (2011).
46. Roth, B. L. Molecular pharmacology of metabotropic receptors targeted by neuropsychiatric drugs. *Nat. Struct. Mol. Biol.* **26**, 535–544 (2019).
47. Roth, B. L., Irwin, J. J. & Shoichet, B. K. Discovery of new GPCR ligands to illuminate new biology. *Nat. Chem. Biol.* **13**, 1143–1151 (2017).

## Methods

**Cloning and molecular biology.** Plasmids containing human Gα constructs were obtained from the cDNA Resource Center (www.cDNA.org), except for Gα12 and GαGustducin, which were synthesized as gene blocks by Integrated DNA Technologies (IDT). Plasmids containing the κOR RASSL Ro1, Gβ2–4 and Gγ1,3–13 were obtained from Addgene, except for Gβ1 and Gγ2-GFP2, which were a gift from M. Bouvier at Université de Montréal. Gα constructs were subcloned into pCDNA5/FRT/TO, and Gβ and Gγ constructs were subcloned into pcDNA 3.1. Receptor constructs were generated by deleting the vasopressin 2 receptor C terminus and tTA sequence from receptor plasmids from the PRESTO-TANGO library[1].

Chimeric constructs (for example, Gα-RLuc8 and Gγ-GFP2 constructs) were generated via HiFi DNA assembly (New England Biolabs). Gγ-GFP2 constructs were generated by amplification of the backbone construct (for example, pcDNA-Gγ) from the N-terminal start codon and adding homology to the C terminus of GFP2 flanked by a short flexible linker sequence (GSAGT). GFP2 sequences were amplified by polymerase chain reaction (PCR), adding homology to the pcDNA backbone at the 5′ end, and homology to the N terminus of the Gγ sequence at the 3′ end. Backbone and insert constructs were co-incubated with HiFi master mix and transformed into Stbl3 *Escherichia coli* (ThermoFisher Scientific). Gα-RLuc8 chimeras were generated by linearizing a single backbone template for each region (for example, the αA-αB linker region, αB-αC helical region and switch III), amplifying outwards from the 5′ and 3′ ends of the beginning of those respective regions, producing a linearized construct lacking that sequence. These deleted codons were filled in with RLuc8 insertion sequences by overhang PCR while adding a flexible SGGGS linker, the missing codon sequences flanking the appropriate insertion site, and homology to the 5′ and 3′ end of the linearized backbone. These were incubated with HiFi master mix to assemble Gα-RLuc8 chimeras containing a fully intact Gα with an RLuc8 sequence, one for each amino acid position within the targeted region. The sequence of each finalized Gα-RLuc8 chimera in the TRUPATH kit is provided in the Supplementary Note.

Pertussis-insensitive Gαi3 (C351I) was generated by PCR mutagenesis.

**Cell culture.** HEK293T cells were obtained from ATCC. HEK293ΔGq/11/12/13/s/Olf cells were a gift from A. Inoue at Tohoku University. Cells were maintained, passaged and transfected in DMEM medium containing 10% FBS, 100 U ml$^{-1}$ penicillin and 100 μg ml$^{-1}$ streptomycin (Gibco-ThermoFisher) in a humidified atmosphere at 37 °C and 5% $CO_2$. After transfection, cells were plated in DMEM containing 1% dialyzed FBS, 100 U ml$^{-1}$ penicillin, and 100 μg ml$^{-1}$ streptomycin for BRET2, calcium and GloSensor assays.

**BRET2 assays.** Cells were plated either in 6-well dishes at a density of 700,000–800,000 cells per well, or 10 cm dishes at 7–8 million cells per dish. Cells were transfected 2–4 h later, using a 1:1:1:1 DNA ratio of receptor:Gα-RLuc8:Gβ:Gγ-GFP2 (100 ng per construct for 6-well dishes, 750 ng per construct for 10 cm dishes), except for the Gγ-GFP2 screen, where an ethanol co-precipitated mixture of Gβ1–4 was used at twice its normal ratio (1:1:2:1). Transit 2020 (Mirus Biosciences) was used to complex the DNA at a ratio of 3 μl Transit per μg DNA, in OptiMEM (Gibco-ThermoFisher) at a concentration of 10 ng DNA per μl OptiMEM. The next day, cells were harvested from the plate using Versene (0.1 M PBS + 0.5 mM EDTA, pH 7.4) and plated in poly-D-lysine-coated white, clear-bottom 96-well assay plates (Greiner Bio-One) at a density of 30,000–50,000 cells per well.

One day after plating in 96-well assay plates, white backings (PerkinElmer) were applied to the plate bottoms, and growth medium was carefully aspirated and replaced immediately with 60 μl of assay buffer (1× Hank's balanced salt solution (HBSS) + 20 mM HEPES, pH 7.4), followed by a 10 μl addition of freshly prepared 50 μM coelenterazine 400a (Nanolight Technologies). After a 5 min equilibration period, cells were treated with 30 μl of drug for an additional 5 min. Plates were then read in an LB940 Mithras plate reader (Berthold Technologies) with 395 nm (RLuc8-coelenterazine 400a) and 510 nm (GFP2) emission filters, at integration times of 1 s per well. Plates were read serially six times, and measurements from the sixth read were used in all analyses. BRET2 ratios were computed as the ratio of the GFP2 emission to RLuc8 emission.

**Calcium mobilization assays.** Cells were plated in 10 cm plates as described in the BRET2 protocol and co-transfected with receptor (1 μg) and Gα-subunit (1 μg) cDNA. The next day, cells were plated at 15,000 cells per well in poly-D-lysine-coated black, clear-bottom 384-well plates (Greiner Bio-One). The following day, growth medium was aspirated and replaced with 20 μl assay buffer containing 1× Fluo-4 Direct Calcium Dye (ThermoFisher Scientific) and incubated for 60 min at 37 °C (no $CO_2$). Plates were brought to room temperature for 10 min in the dark before being loaded into a FLIPR Tetra liquid-handling robot and plate reader (Molecular Devices). Baseline fluorescence measurements were taken for 10 s followed by robotic drug addition (10 μl) and a 60 s measurement (one measurement per second). For antagonist assays, cells were first treated with antagonist and kept in the dark at room temperature for 10 min before agonist addition by the FLIPR Tetra robot. Maximal response during this time was used to calculate the amplitude of the calcium transients. Measurements were analyzed as a percentage of the maximum signal amplitude for the construct.

**GloSensor cAMP assays.** Cells were plated in 10 cm plates as previously described. Cells were transfected with plasmids encoding cDNA for the GloSensor reporter (Promega), receptor and Gα-subunit at a ratio of 2:1:1 (2 μg: 1 μg: 1 μg). The next day, cells were plated in clear-bottom, 384-well white plates. After aspiration of the medium on the day of the assay, cells were incubated for 60 min at 37 °C with 20 μl of 5 mM luciferin substrate (GoldBio) freshly prepared in assay buffer. For Gαs activity, 10 μl of drugs were added using the FLIPR Tetra liquid-handling robot and read after 15 min in a Spectramax luminescence plate reader (Molecular Devices) with a 0.5 s signal integration time. For Gαi activity, 10 μl of drugs was added for a 15 min incubation period. Subsequently, 10 μl of isoproterenol (final concentration of 200 nM) was added and incubated for an additional 15 min period before reading.

**Receptor density measurements.** HEK293T cells were plated in 10 cm dishes and transfected with the μOR and Gαi3 biosensor plasmids according to the BRET2 method detailed above. At 48 h after transfection, membranes for radioligand binding were freshly prepared via hypotonic lysis. Specifically, cells were washed once with 10 ml cold PBS and scraped into 10 ml cold PBS. Cells were collected at 220*g* for 15 min at 4 °C and the supernatant was discarded. The cell pellet was resuspended in 600 μl of cold hypotonic lysis buffer (50 mM Tris HCl, pH 7.4), triturated and aliquoted (100 μl) into 1.5 ml tubes. The crude membranes were collected at 15,000*g* for 30 min at 4 °C. The supernatant was discarded and the membrane pellets were stored at −80 °C.

Receptor density (fmol per mg protein) was measured via homologous competition binding assays in Prism (Graphpad Software). Competition assays were performed in round-bottom 96-well plates (Greiner) using standard binding buffer (50 mM Tris HCl, 10 mM $MgCl_2$, 0.1 mM EDTA, 0.1% fatty acid-free BSA, 1 mM ascorbic acid, pH 7.4) containing two concentrations (~0.8 nM and 3 nM) of [$^3$H]naloxone (70 Ci per mmol, PerkinElmer), serial dilutions of cold naloxone competitor (10 μM to 0.001 nM) and 19.5 mg of μOR + Gαi3 membrane. Pseudo-first-order assumptions were met by using membranes at concentrations that bound <10% of the radioligand added to each well as determined from pilot assays. Non-specific binding was determined in the presence of 10 μM naloxone. Plates were incubated at room temperature in the dark for 1.5 h and a PerkinElmer Filtermate harvester (PerkinElmer) was used to collect membranes onto 0.3% polyethyleneimine-treated GF/B glass fiber filtermats that were washed four times with cold buffer (50 mM Tris HCl, pH 7.4 at 4 °C). The filters were dried, permeated with Meltilex scintillant (PerkinElmer) and counted on a Microbeta plate reader at 1 min per well. Competition curves using different tracer concentrations were simultaneously fitted to the homologous competition equation in Prism (GraphPad) to yield equilibrium dissociation constants ($K_D$) and receptor densities $B_{max}$ (fmol mg$^{-1}$).

**Data analysis.** All concentration–response curves were fit to a three-parameter logistic equation in Prism (Graphpad Software). BRET2 concentration–response curves were analyzed as either raw net BRET2 (fit Emax-fit Baseline) or by normalizing to a reference agonist for each experiment. Efficacy ($E_{max}$) calculations were performed according to ref. [35], and stimulus–response amplitudes (net BRET2) were normalized to the maximal responding agonist (maximal system response). $EC_{50}$ and $E_{max}$ values were estimated from the simultaneous fitting of all biological replicates. Transduction coefficients were calculated as $\log \frac{E_{max}}{EC_{50}}$ as described in ref. [35] and propagation of error was conducted at all steps[48]. $EC_{50}$, $E_{max}$ and transduction coefficient values were analyzed first by analysis of variance (ANOVA) (F-test of curve fit, one-way ANOVA, or two-way ANOVA as described in the text). Post hoc pairwise comparisons used Tukey-adjusted *P* values to control for multiple comparisons. The significance threshold was set at $\alpha = 0.05$.

**Reporting Summary.** Further information on research design is available in the Nature Research Reporting Summary linked to this Article.

## Data availability

All data that were generated or analyzed during this study are included in this Article and its Supplementary Information files or are available from the corresponding authors upon reasonable request. All TRUPATH sensors are available to academic and non-profit institutions as a kit through Addgene (https://www.addgene.org/).

## References

48. Navidi, W. C. *Statistics for Engineers and Scientists* (McGraw-Hill, 2008).

## Acknowledgements

We thank M. Bouvier for the gift of the Gβ1 and Gγ2-GFP2 constructs, T. Kenakin for insights regarding quantitative pharmacology and J. Aubé for the gift of ML139. We also

thank A. Inoue for the donation of the HEK293ΔG cells. Due to space constraints we could not include all citations; for this we apologize.

## Author contributions

R.H.J.O., J.F.D., J.G.E., B.L.R. and R.T.S. developed the concept and designed the experiments. R.H.J.O. and J.F.D. performed the bulk of the molecular biology and experimentation, with A.M.G., B.E.K., S.T.S., T.C., J.D.M., A.C.G. and R.T.S. contributing to the in vitro pharmacology assays. J.G.E. established the cloning strategy and helped with construct generation. R.H.J.O., J.F.D., J.G.E., B.L.R. and R.T.S. wrote and edited the manuscript. This work was supported by NIH grants (nos. R37DA035764, U24DK116195 and RO1MH112205 to B.L.R., KO1MH109943 to R.T.S. and F31NS093917 to R.H.J.O.) and the Michael Hooker Distinguished Professorship to B.L.R.

## Competing interests

R.H.J.O., J.F.D., J.G.E., B.L.R. and R.T.S. are inventors of the TRUPATH technology and could receive royalties. These relationships have been disclosed to and are under management by UNC-Chapel Hill.

## Additional information

**Supplementary information** is available for this paper at https://doi.org/10.1038/s41589-020-0535-8.

**Correspondence and requests for materials** should be addressed to B.L.R. or R.T.S.

**Reprints and permissions information** is available at www.nature.com/reprints.

nature research

Corresponding author(s): Ryan T. Strachan and Bryan L. Roth

Last updated by author(s): Mar 23, 2020

# Reporting Summary

Nature Research wishes to improve the reproducibility of the work that we publish. This form provides structure for consistency and transparency in reporting. For further information on Nature Research policies, see Authors & Referees and the Editorial Policy Checklist.

## Statistics

For all statistical analyses, confirm that the following items are present in the figure legend, table legend, main text, or Methods section.

| n/a | Confirmed | |
|---|---|---|
| ☐ | ☒ | The exact sample size (*n*) for each experimental group/condition, given as a discrete number and unit of measurement |
| ☐ | ☒ | A statement on whether measurements were taken from distinct samples or whether the same sample was measured repeatedly |
| ☐ | ☒ | The statistical test(s) used AND whether they are one- or two-sided<br>*Only common tests should be described solely by name; describe more complex techniques in the Methods section.* |
| ☒ | ☐ | A description of all covariates tested |
| ☐ | ☒ | A description of any assumptions or corrections, such as tests of normality and adjustment for multiple comparisons |
| ☐ | ☒ | A full description of the statistical parameters including central tendency (e.g. means) or other basic estimates (e.g. regression coefficient) AND variation (e.g. standard deviation) or associated estimates of uncertainty (e.g. confidence intervals) |
| ☐ | ☒ | For null hypothesis testing, the test statistic (e.g. *F*, *t*, *r*) with confidence intervals, effect sizes, degrees of freedom and *P* value noted<br>*Give P values as exact values whenever suitable.* |
| ☒ | ☐ | For Bayesian analysis, information on the choice of priors and Markov chain Monte Carlo settings |
| ☒ | ☐ | For hierarchical and complex designs, identification of the appropriate level for tests and full reporting of outcomes |
| ☐ | ☒ | Estimates of effect sizes (e.g. Cohen's *d*, Pearson's *r*), indicating how they were calculated |

*Our web collection on statistics for biologists contains articles on many of the points above.*

## Software and code

Policy information about availability of computer code

| | |
|---|---|
| Data collection | No custom code was used for data collection. All commercial code used for data collection is stated in the methods. |
| Data analysis | No custom code was used for data analysis. All commercial code used for data analysis is stated in the methods. |

For manuscripts utilizing custom algorithms or software that are central to the research but not yet described in published literature, software must be made available to editors/reviewers. We strongly encourage code deposition in a community repository (e.g. GitHub). See the Nature Research guidelines for submitting code & software for further information.

## Data

Policy information about availability of data

All manuscripts must include a data availability statement. This statement should provide the following information, where applicable:

- Accession codes, unique identifiers, or web links for publicly available datasets
- A list of figures that have associated raw data
- A description of any restrictions on data availability

Generated and analyzed data sets that support the findings of this study are available from the corresponding authors upon reasonable request.

# Field-specific reporting

Please select the one below that is the best fit for your research. If you are not sure, read the appropriate sections before making your selection.

☒ Life sciences ☐ Behavioural & social sciences ☐ Ecological, evolutionary & environmental sciences

For a reference copy of the document with all sections, see nature.com/documents/nr-reporting-summary-flat.pdf

# Life sciences study design

All studies must disclose on these points even when the disclosure is negative.

| | |
|---|---|
| Sample size | The number of technical replicates and biological replicates are reported in the main text, figure legends, and tables. Experiments were conducted with at least three biological replicates, but typically ranged between three and fourteen biological replicates. |
| Data exclusions | No data were excluded for this study. |
| Replication | Data were replicated using technical and independent biological replicates. See main text, figure legends, and tables for specific details. |
| Randomization | No data required randomization. |
| Blinding | No data required blinding. |

# Reporting for specific materials, systems and methods

We require information from authors about some types of materials, experimental systems and methods used in many studies. Here, indicate whether each material, system or method listed is relevant to your study. If you are not sure if a list item applies to your research, read the appropriate section before selecting a response.

## Materials & experimental systems

| n/a | Involved in the study |
|---|---|
| ☒ | ☐ Antibodies |
| ☐ | ☒ Eukaryotic cell lines |
| ☒ | ☐ Palaeontology |
| ☒ | ☐ Animals and other organisms |
| ☒ | ☐ Human research participants |
| ☒ | ☐ Clinical data |

## Methods

| n/a | Involved in the study |
|---|---|
| ☒ | ☐ ChIP-seq |
| ☒ | ☐ Flow cytometry |
| ☒ | ☐ MRI-based neuroimaging |

# Eukaryotic cell lines

Policy information about cell lines

| | |
|---|---|
| Cell line source(s) | The HEK293T cell line was sourced from ATCC. HEK293Gq/11/12/13/s/olf null cells (HEK293ΔG) were a generous gift from Dr. Asuka Inoue at Tohoku University, Sendai, Japan. |
| Authentication | All cells used in this study are commercial and were obtained from vendors or sources as indicated in the manuscript. HEK293T were certified by ATCC. HEK293ΔGq/11/12/13/s/Olf null cells were a generous gift from Dr. Asuka Inoue at Tohoku University, Sendai, Japan. |
| Mycoplasma contamination | Cell lines were certified as Mycoplasma-free as they were obtained from the source companies and labs. See Methods for sources. |
| Commonly misidentified lines (See ICLAC register) | No commonly misidentified cell lines were used in this study. |